Journal of Energy Storage 75 (2024) 109748

Contents lists available at ScienceDirect

Journal of Energy Storage

journal homepage: www.elsevier.com/locate/est

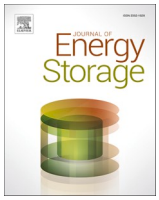

Research papers

Wool/soy protein isolate membranes as separators toward more sustainable lithium-ion batteries

J.P. Serra [a,b], J.C. Barbosa [a,b], M.M. Silva [c], R. Gonçalves [c], J. Uranga [d], C.M. Costa [a,b,*], P. Guerrero [d,e], K. de la Caba [d,e], S. Lanceros-Mendez [a,e,f]

[a] Physics Centre of Minho and Porto Universities (CF-UM-UP), University of Minho, Campus de Gualtar, Braga 4710-057, Portugal
[b] Laboratory of Physics for Materials and Emergent Technologies, LapMET, University of Minho, Braga 4710-057, Portugal
[c] Centre of Chemistry, University of Minho, Braga 4710-057, Portugal
[d] BIOMAT Research Group, University of the Basque Country (UPV/EHU), Escuela de Ingeniería de Gipuzkoa, Plaza de Europa 1, 20018 Donostia-San Sebastián, Spain
[e] BCMaterials, Basque Center for Materials, Applications and Nanostructures, UPV/EHU, Science Park, Leioa 48940, Spain
[f] IKERBASQUE, Basque Foundation for Science, Bilbao 48009, Spain

ARTICLE INFO

Keywords:
Soy protein
Wool
Membrane
Separator
lithium-ion batteries

ABSTRACT

Natural origin products exist in large quantities around the world and many times they are not properly exploited in order to realize their potential in novel applications, being often even discarded as by-products from other uses. In this study, wool and soy protein isolate (SPI) are proposed to develop separator membranes for lithium-ion batteries (LIBs), aiming toward a new generation of sustainable batteries. The developed membranes show suitable wettability by the electrolyte solution and are characterized by a porous morphology that becomes more irregular with the addition of wool with respect to the distribution and size of the pores. The physicochemical properties of the membranes are not strongly affected by the addition of wool, excepting for the low mechanical resistance of the SPI membranes, which is improved with the presence of wool. With respect to lithium-ion battery applications, the ionic conductivity is larger than 10^{-4} S.cm^{-1} and the lithium transference number ranges between 0.42 and 0.67, leading to excellent battery performance with a discharge capacity up to ~150 mAh.g^{-1} at C/10 rate. Overall, the developed membranes represent a suitable alternative to conventional LIB separators taking into account the need for environmental friendlier approaches compatible with a circular and sustainable economy.

1. Introduction

Several global problems in the world must be urgently addressed to guarantee the quality of life for future generations [1]. Among them, energy represents one of the biggest ones, based on its impact in industry, transportation, wellbeing as well as on the related environmental impact of current energy types and technologies. The increase in human population and in quality of life leads to a larger demand for energy [2]. In turn, the continuous development of industry, together with the consumption of non-renewable resources, such as fossil fuels, led to severe environmental impact [3].

A set of goals were defined for the countries in order to avoid the increasing environmental impacts and achieve a sustainable society [4]. Within the various objectives, the commitment to renewable energy sources was set [5], which together with energy storage systems, such as batteries, will allow more sustainable energy production and consumption [6]. In this context, the demand for lithium-ion batteries (LIBs) has grown significantly over the last years, related to the development of small electronic devices as well as with the transition from fossil fuel-based mobility toward the electric vehicle [7]. Batteries are electrochemical systems that convert chemical energy into electrical energy and vice-versa through oxidation-reduction reactions. They are made up of two electrodes (the cathode and the anode) and between them there is a porous membrane (separator) immersed in an electrolyte solution [8]. The electrodes are formed by three components: an active material, a conductive material and a polymer binder [9]. In the case of the cathode, which is responsible for the battery capacity, different active materials have been developed, including lithium iron phosphate, LFP [10], lithium manganese oxide, LMO [11], and lithium cobalt oxide, LCO [12], among others. The anode has the function of receiving and storing

* Corresponding author at: Physics Centre of Minho and Porto Universities (CF-UM-UP), University of Minho, Campus de Gualtar, Braga 4710-057, Portugal.
E-mail address: cmscosta@fisica.uminho.pt (C.M. Costa).

https://doi.org/10.1016/j.est.2023.109748
Received 17 July 2023; Received in revised form 3 November 2023; Accepted 13 November 2023
Available online 18 November 2023

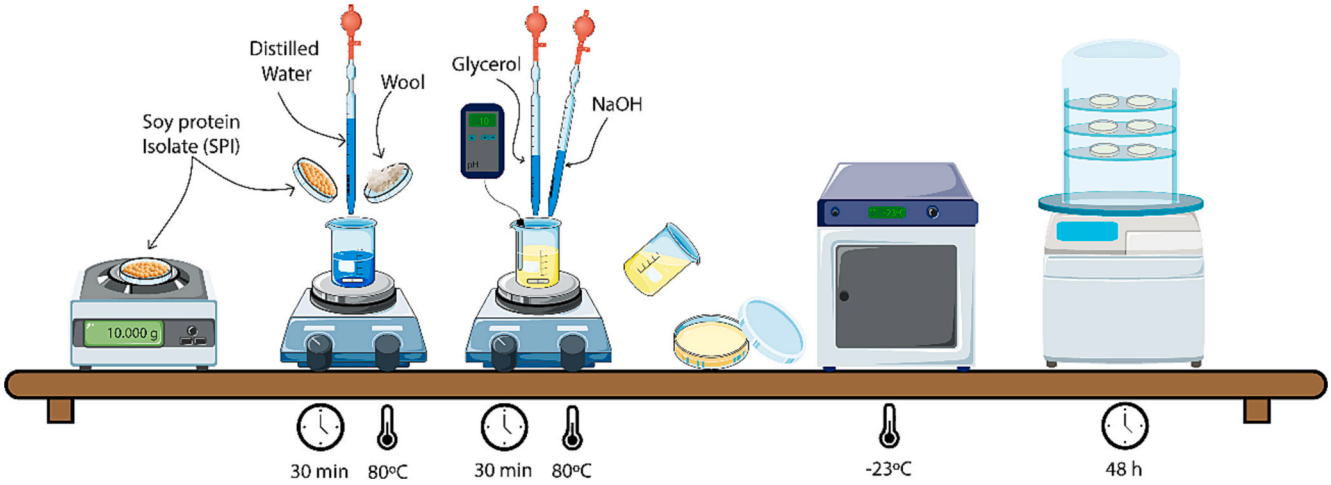

Fig. 1. Schematic representation of membrane preparation and conditions.

lithium and some of the most used materials include graphite and graphene [13] and silicon [14]. The separator membrane is made up of a polymeric matrix generally of synthetic origin, such as poly(vinylidene fluoride), PVDF, and its co-polymers [15], polyethylene oxide, PEO [16], or polypropylene, PP [17], among others. The search for more sustainable alternatives for the current separators led to some alternatives, including as the development of solid polymer electrolytes, which currently still lack performance and durability [18–20], and the use of polymers from natural and renewable resources. In this context, research in the field of novel battery separators, based on renewable raw materials, has become a challenge for the replacement of traditional commercial polyolefin-based separators [21].

Polymers derived from natural and renewable resources show large potential to develop separator membranes thanks to their availability, biodegradability, non-toxicity and compliance with the circular-economy principles [22]. Within this perspective, materials of natural origin that have been used for separator membrane development include silk [23], carrageenan [24], sodium alginate [25], poly (L-lactic acid) [26], cellulose [27], or chitin [28], among others. Currently the focus is on giving value to waste polymeric materials from different industries, giving these materials a second life of added value and leading to more sustainable batteries. Among them, soy protein isolate (SPI), obtained as by-product from soy oil production, can be a good candidate for battery applications due to the polar groups present in this protein, which are able to adsorb and desorb ions [29]. Likewise, the polar groups in the wool chains, including amine, thiol and carboxyl groups [30], make wool suitable in this field of application. Considering that the current worldwide wool production is around 1.16 million tons/year (clean wool), from which 10–15 % fiber is wasted during cleaning and 12–15 % waste is produced during its transformation from yarn to fabric [31], the utilization of wool in the preparation of separators would be a good strategy to revalorize these underutilized wastes.

In this work, we show the development of new battery separator membranes based on SPI with different amounts of wool through the freeze-dried process, where the morphological, physicochemical, mechanical and electrochemical properties were evaluated. In addition, the battery performance of this separator was carried out on half cathode cells. The focus is the valorization of waste materials for added value energy applications.

2. Materials and methods

2.1. Materials

The separator membranes were prepared using soy protein isolate (SPI) PROFAM 974 (ADM Protein Specialties Division, The Netherlands), wool from latxa sheep, supplied by Landazurieta farm in Ametzaga de Zuia (Araba), and glycerol (purity of 99.01 %, Panreac, Spain). All chemicals were utilized as received without further purification. Lithium hexafluorophosphate in a mixture of ethyl carbonate (EC) and dimethyl carbonate (DMC) (1:1 in vol. ratio), ($LiPF_6$ in EC: DCM, Sigma-Aldrich, Spain) was used to assess the electrolyte uptake.

2.2. Preparation of the membranes

Freeze-drying technique was used to prepare SPI and wool containing membranes. Prior to use, wool was cut into small pieces. Then, 10 g of SPI were mixed with 0, 5, 15, or 25 wt% wool (on SPI dry basis) in 125 mL of distilled water, and mixtures were heated at 80 °C under continuous stirring for 30 min considering that, above of 25 wt% of wool, the membranes are more brittle. After that, 30 wt% glycerol (on SPI dry basis) was added and NaOH (1 $mol.dm^{-3}$) was employed to adjust solution pH to 10. The mixture procedure was repeated, heating solutions at 80 °C for other 30 min under continuous stirring (Ika, model no. C-MAG HS 7). Mixtures were poured into a multiwell plate, cooled down at room temperature and put into a freezer at −23 °C (Alpha 1–4 LDplus freeze-drier, Thermo Fisher). Finally, membranes were freeze-dried for 48 h (Alpha 1–4 LSC basic) and taken out from the wells. The obtained membranes show thickness from 30 to 60 mm depending on the wool content. In the following, the membranes are designated as control, SPI5W, SPI15W and SPI25W, as a function of the wool content, 0, 5, 15 and 25 %, respectively. The preparation of the Wool/SPI membranes is represented in Fig. 1.

2.3. Characterization of the membranes

2.3.1. Morphology, porosity and density evaluation

Hitachi S-4800 field emission scanning electron microscope, SEM (Hitachi High-Technologies Corporation), with accelerating voltages of 5 kV was used to observe the morphology of the membranes. Samples were stuck onto a metal stub by a double-side adhesive tape and sputtered-coated (JFC-1100) under vacuum with a thin layer of gold in an argon atmosphere prior to observation. The porosity was quantified by PoreMaster GT-60 Mercury-intrusion apparatus (Quantachrome Instruments), equipped with low-pressure (0.1 psi) and high-pressure (60,000 psi) devices. Before testing, membranes were dried at 105 °C for 12 h and then, the density was measured in an automatic He Microultra Pycnometer (Quantachrome Instruments).

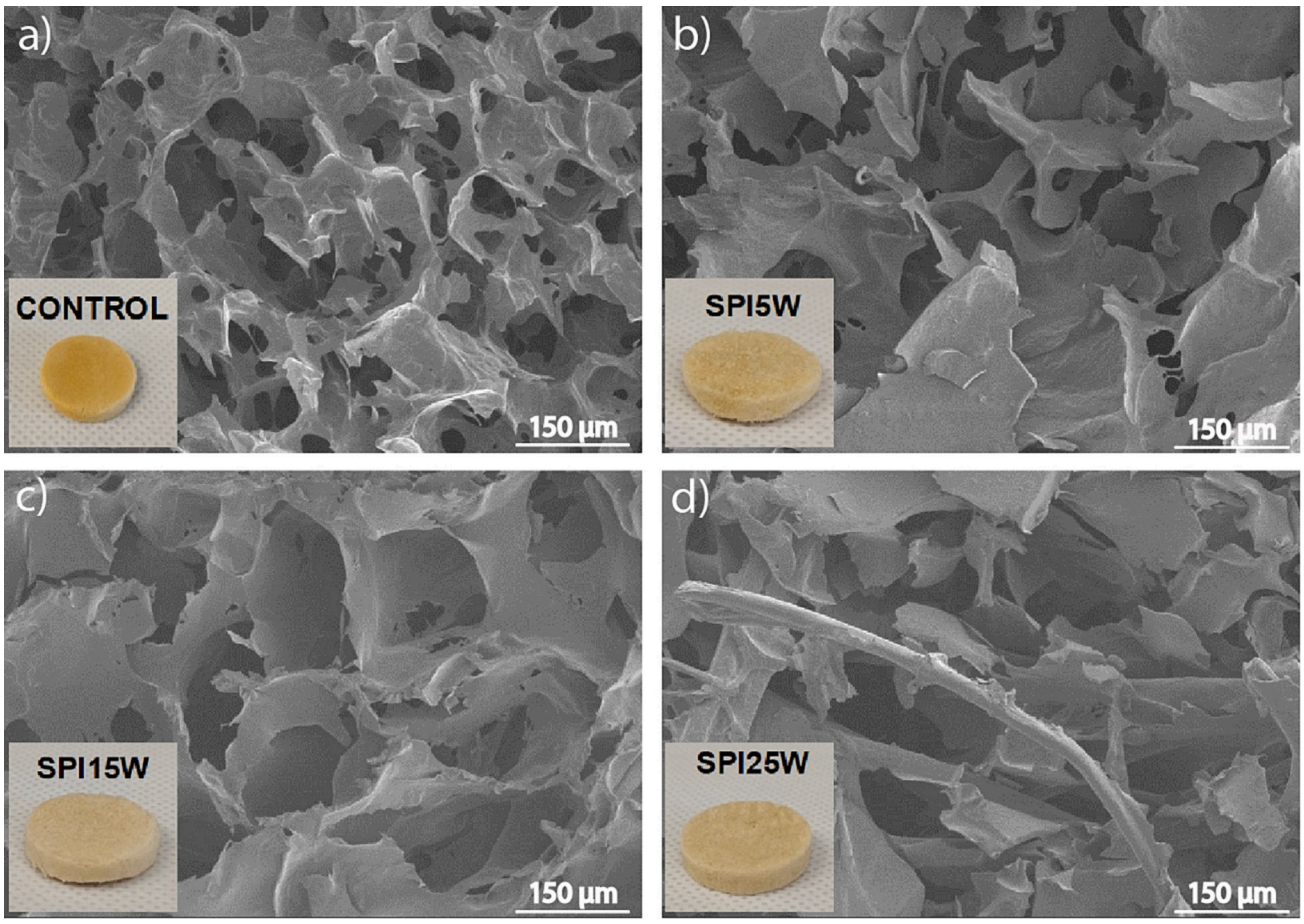

Fig. 2. SEM images for wool/SPI membranes.

2.3.2. Structural evaluation

X-ray diffraction, XRD, patterns were recorded in a PANalyticXpert PRO diffractometer by using Cu-Kα ($\lambda = 1.5418$ Å) radiation source at a generator voltage of 40 kV and a generator current of 40 mA. 2θ values ranged from 2 to 50°, where θ is the incidence angle of the X-ray beam on the sample. The XRD analysis of the membranes was taken before and after electrolyte uptake to study the influence of electrolyte into the membrane structure.

Wool/SPI samples were analysed by Fourier transform infrared (FTIR) spectroscopy before and after the electrolyte uptake using a Platinum-ATR Alpha II FTIR spectrometer (Bruker). A spectral resolution of 4 cm^{-1} was used and 32 scans were acquired for each spectrum. All spectra were recorded within the range from 4000 to 800 cm^{-1}.

2.3.3. Puncture strength

Puncture strength was evaluated using a TA.XT.Plus C Texture Analyzer (Aname Instrumentación Científica), equipped with a 5 kg load cell. Membranes were perforated with a spherical probe of 5 mm diameter. Data were collected at 3 mm/s speed. All samples were conditioned at 100 % humidity for 48 h before testing.

2.3.4. Thermal evaluation

Thermal stability of wool/SPI membranes was assessed by thermogravimetric analysis, *TGA*, using a Mettler Toledo TGA SDTA 851 equipment (Mettler Toledo S.A.E.). Samples were heated from 25 to 800 °C at 10 °C.min^{-1} under nitrogen atmosphere (10 mL/min). TGA and the derivative form of TGA (DTG) data were assessed.

The thermal characteristics of the samples were evaluated also by differential scanning calorimetry, DSC, in a Mettler Toledo DSC 822. The samples (3.0 ± 0.2 mg) were sealed in aluminium pans and heated from −50 to 260 °C at 10 °C.min^{-1} in an inert environment (10 mL N_2/min).

2.3.5. Electrolyte uptake and electrochemical parameters

Membranes were weighed (w_i) in an analytic balance (A&D Instruments, cat. no. GR-200), immersed into the electrolyte and weighed again after specific times of immersion (w_t). The electrolyte uptake was determined as follows:

$$Electrolyte\ uptake\ (\%) = \frac{w_t - w_i}{w_i} \cdot 100 \quad (1)$$

The main electrochemical parameters for battery operation were analysed taking into account ionic conductivity (σ_i), electrochemical stability window and Li-ion transfer number (t_{Li}^{+}). The ionic conductivity of the different SPI membranes with wool was calculated after testing the wettability of the samples in the electrolyte solution (uptake process) through electrochemical impedance by placing the membrane between 2 gold electrodes with 10 mm diameter. This system was placed inside a Buchi TO51 and the impedance was evaluated at room temperature in an Autolab PGSTAT-12 by varying frequency between 500 mHz and 500 kHz with a signal of 10 mV. The ionic conductivity value was calculated by the following expression:

$$\sigma_i = \frac{d}{R_b \times A} \quad (2)$$

where d is the thickness of the separator sample, R_b is the bulk resistance and A is the electrode area.

The electrochemical stability window of the different samples was evaluated using a two-electrode cell system (25 µm diameter gold microelectrode and lithium metal) at room temperature. Measurements were performed in a glow box filled with argon with an Autolab

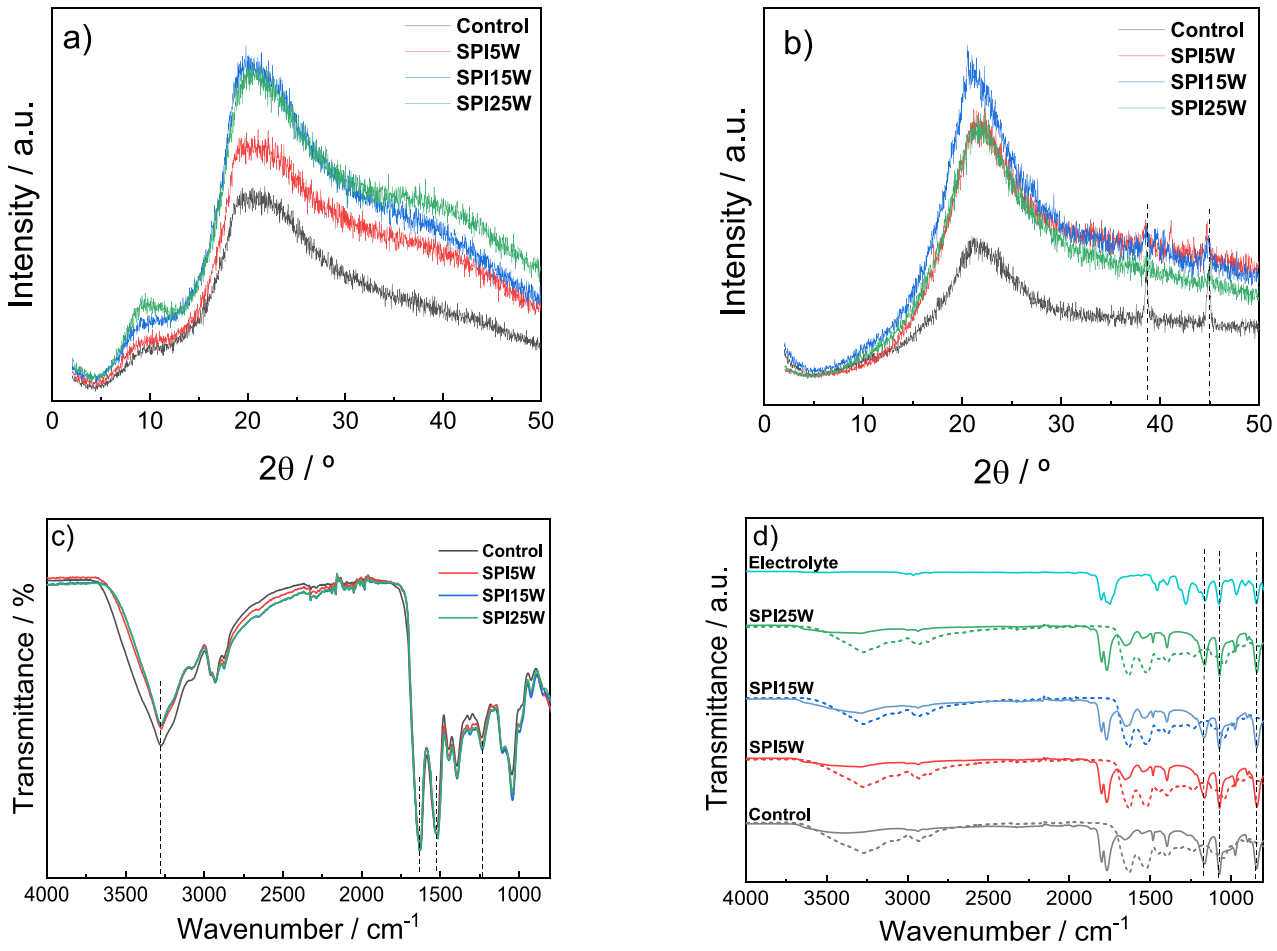

Fig. 3. XRD patterns of wool/SPI membranes: a) before and b) after electrolyte uptake. FTIR spectra of wool/SPI membranes: c) before the electrolyte uptake and d) before (dots) and after (line) the electrolyte uptake, together with the electrolyte spectrum.

PGSTAT-12 with a sweep speed of 0.1 $V.s^{-1}$.

The lithium transfer number (t_{Li}^{+}) was calculated by placing the developed membranes between two lithium metal electrodes in a Swagelok cell. The value was calculated using potentiostatic polarization applying a DC voltage of 10 mV using Eq. (3):

$$t_{Li+} = \frac{I^s[\Delta V - I^0 R^0]}{I^0[\Delta V - I^s R^s]} \quad (3)$$

where I^s and I^0 are the steady and initial currents, respectively, ΔV is the applied potential, and R^0 and R^s are the initial and final resistances of the Li electrode/electrolyte before and after polarization, respectively.

2.3.6. Batteries preparation, assembly and characterizations

Wool/SPI membranes were tested by mounting cathodic half cells with the configuration (lithium metal, wool/SPI separator, LFP cathode) in a glove box with an inert atmosphere of argon. All the samples for the assembly of the half-cells were previously dried at 60 °C under vacuum overnight in a Buchi oven and pressed at 50 $kg.cm^2$ for 2 min in order to reduce thickness.

LFP cathodes were prepared with a ratio of 80:10:10 of active material, conductive material and a polymer binder, respectively. The cathodic ink was spread in an aluminium foil, which works as current collector, as reported in [32].

The half-cells were tested in charge and discharge cycles at different rates (C/10, C/5, C/2, C and 2C) with 10 cycles each rate. The life performance was valuated after 100 cycles at C and 2C. Discharge capacity values were recorded using Landt CT2001A instrument. Finally, half-cells were measured by impedance spectroscopy before and after battery cycling tests. The measurements were carried with an Autolab PGSTAT12 instrument in the frequency range from 10 mHz to 500 kHz and with a signal amplitude of 10 mV.

3. Results and discussion

3.1. Morphological and physicochemical properties

A high porosity of the samples typically allows effective electrolyte uptake and retention, which is essential for battery applications [33]. Since the separator performance is strongly influenced by the movement of ions in the separator and this movement is closely related to the separator pore size and distribution, these properties were assessed for wool/SPI membranes (Fig. 2). The results show that the control membranes revealed more defined and uniform pores, whereas wool containing samples had randomly distributed pores of varying sizes and shapes, increasing tortuosity with wool content increase. The membrane porosity was calculated by mercury-intrusion apparatus and a porosity of 83 % was obtained for the control membrane, which remained similar for the wool containing membranes. Separators with sub-micron pore sizes have been proven to be adequate to prevent the internal short circuits since the tortuous structure of the pores assists in blocking dendrites from reaching the opposite electrode [34]. Additionally, the typical slit-like pore structures of poly(propylene) PP separators that lead to poor electrolyte retention property [35] were not present in the developed wool/SPI membranes.

Concerning XRD analysis, samples exhibited two reflections peak

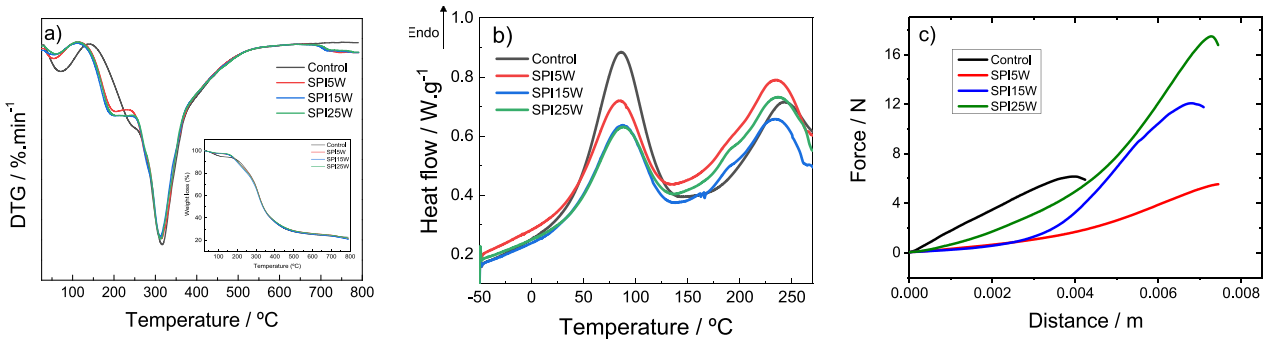

Fig. 4. a) DTG curves, b) DSC thermograms and c) puncture force vs distance for wool/SPI membranes.

centered at about 9° and 20° (Fig. 3a)), related to α-helix and β-sheet secondary conformations of SPI and wool keratin chains, respectively [36]. After the addition of wool, the intensity of the peak associated to the β-sheet conformations increased in comparison to that of the control membrane. Moreover, as wool content increased, this reflection intensity increased due to the interactions among the different membrane components. Regarding the membranes immersed into the electrolyte (Fig. 3b)), new reflection peaks appeared around 39–45°, which can be attributed to lithium hexafluorophosphate [37], indicating effective electrolyte uptake. Also, reflection peaks at about 9° related to the α-helix secondary conformations of SPI is substantially reduced, inducing higher lithium-ion mobility through the β-sheet [38].

FTIR spectra of wool/SPI membranes before immersion into the electrolyte are shown in Fig. 3c), where the typical absorption bands of SPI and keratin, the wool main component, can be distinguished. All spectra showed strong bands around 3500–3000 cm^{-1}, corresponding to the hydroxyl and amino groups [39]. Moreover, protein characteristic bands at 1630 cm^{-1} (amide I), 1520 cm^{-1} (amide II) and 1232 cm^{-1} (amide III), which correspond to the C═O stretching vibrations, to the coupling of N—H bending and C—N stretching, and to the C—N stretching coupled with plane N—H bending, respectively, were observed [40]. The intensity of the band ranging from 3000 to 3500 cm^{-1} in wool/SPI samples decreased compared to that of the control sample, indicating the decreased stretching of free hydroxyl bonds, which might be caused by the formation of intermolecular hydrogen bonding between SPI and wool keratin. Otherwise, the spectra showed no wavenumber displacements of the bands with the addition of wool, irrespective of wool content; hence, there was no chemical reaction between the formulation components.

Additionally, Fig. 3d) presents the FTIR spectra of wool/SPI membranes before and after electrolyte uptake, together with the electrolyte spectrum. Some differences can be observed between the membranes without and with the electrolyte, mainly the presence of bands corresponding to the electrolyte, which appear around 1800, 1760, 1160, 1070 and 840 cm^{-1}. Moreover, band intensity changes occurred because of new physical interactions between the membranes and the electrolyte. Particularly, the reduced band intensity of amide I at 1630 cm^{-1}, indicated a lower α-helix conformations, result also verified by XRD analysis [41]. In this regard, an effective electrolyte uptake can be confirmed, separators exhibiting the necessary chemical resistance to the electrolyte.

3.2. Thermal and puncture resistance

Thermal stability is also a critical characteristic for the long-time use of LIBs exposed to harsh conditions. The thermal properties of wool/SPI membranes were assessed by TGA and DSC analyses. Regarding TGA (Fig. 4a)), the weight loss before 100 °C was related to the removal of moisture from the membranes. During the second degradation step (around 200 °C), T_{max} slightly changed when wool was added; in fact, this mass loss is mainly associated to the evaporation of glycerol [42],

Table 1
Maximum force, rupture energy, ionic conductivity and lithium-ion transference number for wool/SPI membranes.

	Maximum force (N)	Rupture energy (mJ)	Ionic conductivity (mS. cm^{-1})	t_{Li+}
Control	5.82 ± 0.34	13.30 ± 0.81	–	–
SPI5W	6.05 ± 0.21	16.10 ± 0.86	1.60	0.42
SPI15W	10.12 ± 0.33	25.20 ± 0.84	1.22	0.50
SPI25W	16.46 ± 0.53	47.12 ± 1.75	1.93	0.67

but also to the initial wool degradation. Wool commonly undergoes several pyrolysis consequences from 200 to 400 °C, including the rupture of peptide helical structure, a solid to liquid transition, and breakage of disulphide links [31]. Thereby, the third weight loss stage, appearing around 315 °C, may be attributed to the wool degradation as well as to the soy protein peptide bond degradation, which results in a large mass loss [43]. It is worth noting that wool/SPI membranes showed outstanding thermal resistance compared to PP separators, which melt at 150–165 °C [44].

Regarding DSC analysis (Fig. 4b)), the first thermal event was detected at around 100 °C, attributed to water evaporation together with the denaturation of β-conglycinin (7S) [45]. Water interacts with proteins and facilitates protein denaturation, decreasing denaturation temperatures [46]. However, intermolecular hydrogen bonding between SPI and wool keratin hinders interactions with water, leading to lower moisture content in wool containing samples. Consequently, the β-conglycinin denaturation temperature increases slightly from 85 °C for the control sample to 88 °C for the SPI25W sample. Further, there is also a decrease in the enthalpy required for protein denaturation, which changes from 187 $J.g^{-1}$ for the control sample to 96 $J.g^{-1}$ for the SPI25W sample. At higher temperatures, between 220 and 250 °C, another peak is observed for all samples, related to the melting of α-keratin crystals, together with the denaturation of glycinin (11S) [47]. Since these endothermic peaks are associated, among others, with the presence of keratin in wool, the enthalpy required for protein denaturation increases from 61 $J.g^{-1}$ for the control sample to 78 $J.g^{-1}$ for SPI25W sample and, consequently, there is a slight decrease in denaturation temperature from 243 °C for the control sample to 236 °C for SPI25W.

Since sharp crystalline phases, known as lithium dendrites, are created during battery cycling and they are among the main causes of physical separator failure, puncture strength was used to measure the mechanical resistance. As presented in Fig. 4c), the puncture strength of the membranes was improved with increasing wool content, since puncture occurred at higher force values for SPI15W and SPI25W membranes with respect to the control sample. In particular, the SPI25W membrane exhibited significant differences in maximum force values (16.46 and 5.82 N) and rupture energies (47.12 and 13.30 mJ) in comparison to the control membrane, as shown in Table 1. Therefore, it can be concluded that the addition of wool promoted the formation of

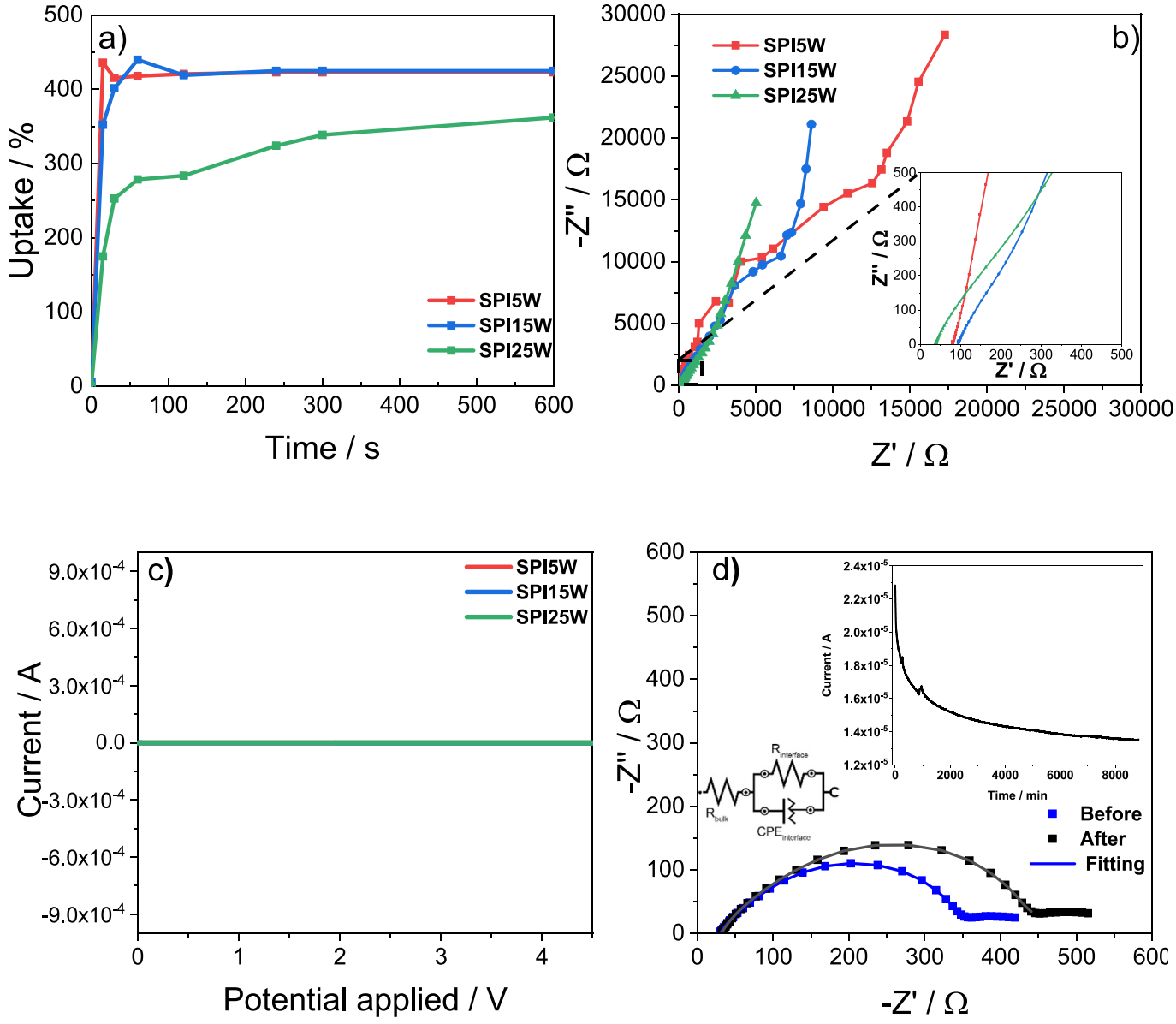

Fig. 5. a) Electrolyte uptake and b) Nyquist plot of the wool/SPI separators. c) Cyclic voltammogram and d) DC polarization measurements for the wool/SPI membranes.

more resistant networks. In fact, high specific strengths and stiffnesses of some natural fibers provide benefits for mechanical performance and, more specifically in the case of wool, the complex structure of the microfibril-matrix plays a relevant role to improve mechanical properties [48]. Nevertheless, all samples showed suitable values for battery applications, since the puncture strength of a separator membrane should be higher than 2.9 N [44].

3.3. Electrochemical characteristics

After analysing the physicochemical, thermal and mechanical characteristics, samples were subjected to electrochemical tests to understand the performance of these membranes as LIB separators. The soy protein sample without wool was not assessed since this control sample presents a brittle nature without the necessary mechanical properties for this application.

A critical property of separator membranes is the electrolyte uptake. A battery separator should exhibit a large electrolyte uptake capacity toward adequate compatibility with the ion-conducting media. One of the parameters initially analysed was the wettability of the separator membranes, adjusted to the battery size, to the electrolyte solution through the uptake process and the results are shown in Fig. 5a), where a rapid absorption of the electrolyte is observed, reaching equilibrium in <1 min. The SPI5W and SPI15W samples show similar values of mass increase when wetted in the electrolyte, in the order of 420 %, while the SPI25W membrane presents a lower uptake value, in the order of 330 %, being still possible to observe that the electrolyte absorption of this sample is slower, reaching stability after 240 s. These values are due to the high porosity of the samples; however, a higher concentration of wool affects the wettability of the membrane by the electrolyte solution.

Fig. 5b) presents one of the main relevant parameters for the use of these materials as LIB separators, the ionic conductivity, which was evaluated after the electrolyte uptake process. The ionic conductivity of wool/SPI membranes was calculated through impedance spectroscopy, as shown in the Nyquist plots of Fig. 5b), and using Eq. (2). The Nyquist plots show straight line which increases with increasing frequency and corresponds to the ion diffusion process [49]. The ionic conductivity values of each sample are reported in Table 1 and are within the

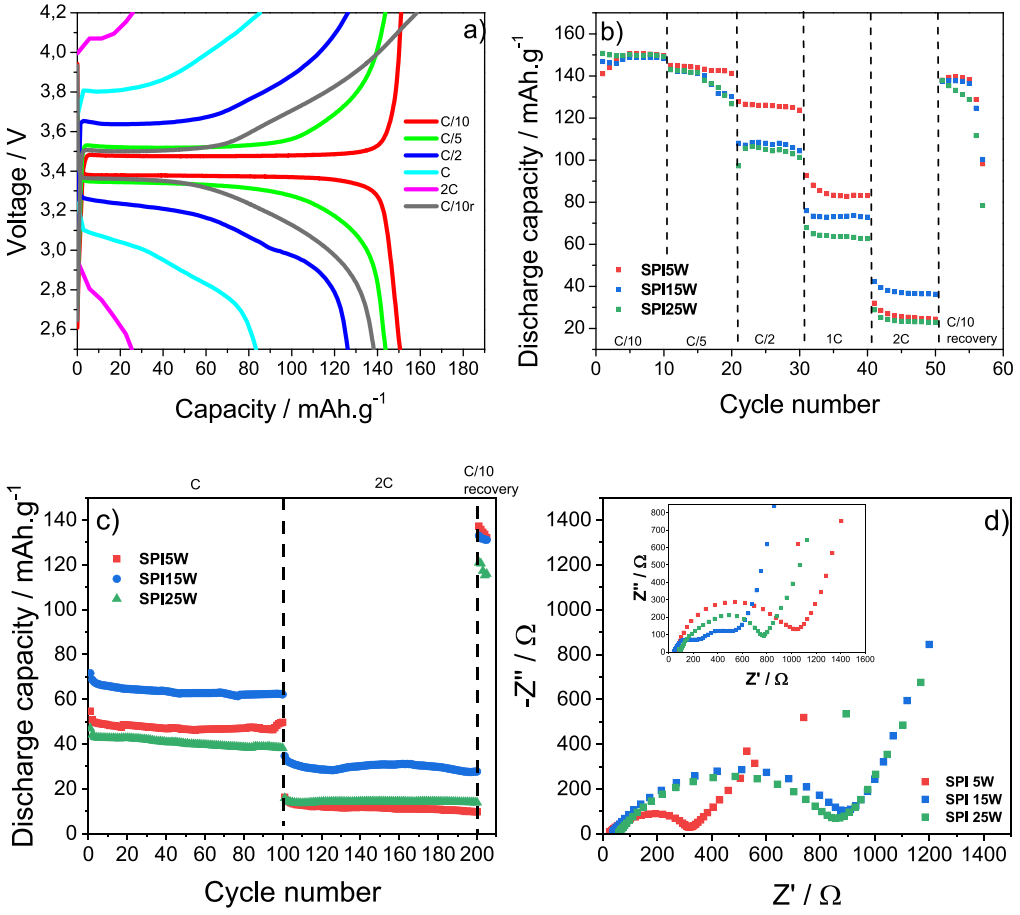

Fig. 6. a) Charge/discharge profiles for the cathodic half-cells for the wool/SPI membranes (SPI5W), b) rate performance as a function of the cycle number with the different wool/SPI membranes, c) discharge capacity value at C and 2C rate for 100 cycles for wool/SPI half-cells and d) electrochemical impedance spectroscopy: before and after (inset) cycling of the half-cell batteries prepared with the wool/SPI membranes as separator.

established values considered suitable for the operation of the membranes as separators of lithium-ion batteries (10^{-4} S.cm^{-1}) [50].

The electrochemical stability of the materials is also a relevant parameter for battery applications, since they are subject to variations in constant voltage ranges between each charge and discharge cycle and any reaction of the materials to these voltage changes in the system can lead to fatigue of the material after a few cycles, compromising the viability of this material in its application. Fig. 5c) presents a cyclic voltammogram between 0.0 and 5.0 V for each of the samples and shows that, regardless of the different membranes developed, none of them presents any anodic or cathodic peak, demonstrating that these samples are stable in the normal operating voltage range of batteries with LFP as cathode (2.5 to 4.2 V).

The Bruce and Evans method allows calculating the lithium-ion transfer number (t_{Li+}). This value varies between 0 and 1 and it is desirable to be as close to 1 as possible for battery applications. The obtained results are characterized by the impedance evaluation before and after the chronoamperometry measurement. This evaluation shows an increase in the internal resistance of the system from 335 to 440 Ω, indicating an increase in the interfacial resistance of the symmetrical cell [51]. Fig. 5d) shows the lithium-ion transfer graphs of the sample with the best performance in this parameter (SPI25W) and, in Table 1, the corresponding t_{Li+} values, which increase with increasing wool content in the samples, are shown.

3.4. Battery performance

Taking into account the results obtained in Fig. 5, the developed samples were tested as separators of LIBs. The membranes were assembled and evaluated in charge and discharge tests at different C-rates at room temperature. Ten cycles were performed for each C-rate. Fig. 6a) shows the typical behaviour of the charge and discharge profiles at the fifth cycle of the different rates (C/10, C/5, C/2; C, 2C and C/10 recovery), when C-LFP is used as cathode. These profiles are due to the removal of lithium in the charging process and the insertion of lithium in the discharge process and rearrangements in the cathodic structure of the half-cells. This behaviour decreases with increasing C-rate due to ohmic polarization. The cycling behaviour of the different wool/SPI membranes at different cycling rates shows that the discharge capacity value of the SPI5W membrane is 150 mAh.g^{-1}, 143 mAh.g^{-1}, 126 mAh.g^{-1} 83 mAh.g^{-1} 25 mAh.g^{-1} and 138 mAh.g^{-1} at the C rates of C/10, C/5, C/2, C, 2C and C/10.

Fig. 6b) shows the rate performance of the different samples developed (10 charge-discharge cycles for each rate), showing the discharge capacity as a function of the number of cycles. It is observed that for the C/10 rate the samples show similar values in the order of 150 mAh.g^{-1}. Relevant differences appear in the following rates and in all rates (except 2C). The battery that has the best discharge capacity is the one with SPI5W as separator membrane.

Fig. 6c) presents the cycle life performance of the batteries at a rate of C and 2C over 100 cycles. A higher discharge capacity for the SPI15W sample is observed when compared with the rest of the samples, presenting a discharge capacity value around 72 and 62 mAh.g^{-1} and 35 and 28 mAh.g^{-1} for the first and last cycle at rate C and 2C, respectively, representing a capacity fade of 13 and 20 % after 100 cycles for the rates mentioned before. SPI5W and SPI25W samples present a similar

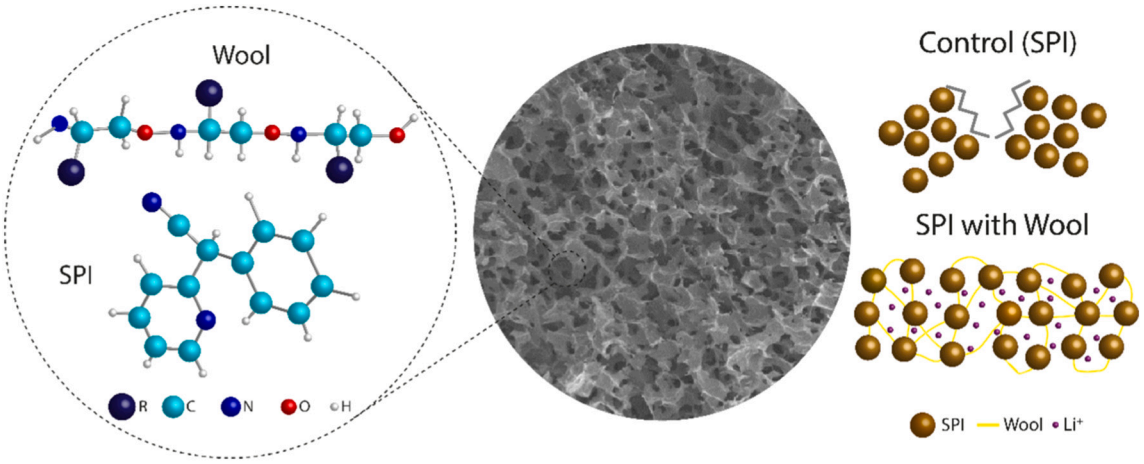

Fig. 7. Schematic representation of interaction mechanisms in the wool/SPI samples.

behaviour between them for the 2C rate, showing a similar discharge capacity value for the first cycle (around 16 mAh.g^{-1}). However, the SPI5W sample presents a higher capacity fade over cycling when compared with SPI25W (40 and 12 % for SPI5W and SPI25W, respectively). These are excellent results for a natural polymer, particularly regarding the high applied discharge rates (1C and 2C) for a prolonged number of cycles.

Finally, the electrochemical impedance of half-cell batteries before and after cycling was evaluated, and the results are presented in Fig. 6d). All Nyquist plots are characterized by a double semicircle followed by a linear region and the semicircles represent the half-cell system resistances (electrolyte, interfacial and charge transference resistances). Before the cycling process, the SPI5W sample presents a lower resistance when compared with the other samples, which proves the best performance of this membrane in the charge-discharge tests (Fig. 6d). After the cycling process, an increase in resistance is observed, attributed to the formation of solid electrolyte interface layer (SEI).

In conclusion, the developed sustainable membranes can be used as LIB separators and the membrane with the best performance was the sample with SPI and 15 wt% of wool. It is proved that, despite the ordered porous structure of SPI sample, it presents a fragile nature lacking the necessary mechanical properties for a LIB separator. However, the introduction of a small amount of wool acts as a mechanical reinforcement of the porous membrane, leading to a tortuous porous structure with improved battery performance (Fig. 7). Also, this behaviour is verified through the interaction between of wool content of electrolyte solution observed from XRD and FTIR analysis.

4. Conclusions

The development of sustainable batteries based on products of natural origin, such as soy protein isolate and wool, for lithium-ion battery separators becomes essential taking into account environmental and circular economy considerations. In this work, soy protein isolate, SPI, was used with different amounts of wool up to 25 wt% content, and membranes were prepared through the freeze-drying method. The porosity of the different samples remains more or less constant (>80 %) despite the addition of wool, which leads to more irregular pores, both in size and shape. Through the swelling process, an excellent wettability is detected between the electrolyte solution and the samples, and it is also verified that the vibration bands and the thermal properties are not strongly affected by the addition of wool, the membranes being stable up to temperatures around 150 °C. The addition of wool gives the SPI membranes a superior mechanical resistance when compared to the control. Regarding the electrochemical data, ionic conductivity and lithium transfer number presented values between 1.22 and 1.93 mS. cm^{-1} and 0.42 and 0.67, respectively, for the samples with different wool content. All cathodic half-cells show an excellent electrochemical performance at different C-rates with particular emphasis on the membrane with 15 wt% wool content, that presents a higher discharge capacity value when compared with other samples. Cycle life performance at 2C rate is also verified with a discharge capacity value of 28 mAh.g^{-1} for SPI15W and 130 mAh.g^{-1} at C/10 after 100 cycles. This study demonstrates that it is possible to develop sustainable lithium-ion batteries separators based on soy protein isolate and wool.

CRediT authorship contribution statement

J.P. Serra: Methodology, Validation, Formal analysis, Investigation, Writing – original draft, Writing – review & editing. **J.C. Barbosa:** Methodology, Validation, Formal analysis, Investigation, Writing – original draft, Writing – review & editing. **M.M. Silva:** Methodology, Validation, Formal analysis, Investigation, Writing – original draft, Writing – review & editing. **R. Gonçalves:** Methodology, Validation, Formal analysis, Investigation, Writing – original draft, Writing – review & editing. **J. Uranga:** Methodology, Validation, Formal analysis, Investigation, Writing – original draft, Writing – review & editing. **C.M. Costa:** Methodology, Validation, Conceptualization, Formal analysis, Investigation, Writing – original draft, Writing – review & editing. **P. Guerrero:** Methodology, Resources, Conceptualization, Investigation, Validation, Project administration, Writing – original draft, Writing – review & editing. **K. de la Caba:** Methodology, Validation, Conceptualization, Project administration, Formal analysis, Investigation, Writing – original draft, Writing – review & editing. **S. Lanceros-Mendez:** Methodology, Resources, Funding acquisition, Conceptualization, Validation, Investigation, Project administration, Writing – original draft, Writing – review & editing.

Declaration of competing interest

The authors declare that they have no known competing financial interests or personal relationships that could have appeared to influence the work reported in this paper.

Data availability

Data will be made available on request.

Acknowledgments

The authors thank the Fundação para a Ciência e a Tecnologia (FCT) for financial support under the framework of Strategic Funding UIDB/

04650/2020, UID/FIS/04650/2020, UID/EEA/04436/2020, and UID/QUI/00686/2020 and under POCI-01-0247-FEDER-046985 and 2022.03931.PTDC funded by national funds through FCT and by the ERDF through the COMPETE2020—Programa Operacional Competitividade e Internacionalização (POCI). NGS-New Generation Storage, C644936001-00000045, supported by IAPMEI (Portugal) with funding from European Union NextGenerationEU (PRR).The authors also thank the FCT for financial support under Grant 2021.08158.BD (J.P.S.), SFRH/BD/140842/2018 (J.C.B.) and FCT investigator contracts CEECIND/00833/2017 (RG) and 2020.04028.CEECIND (C.M.C.). This study forms part of the Advanced Materials program and was supported by MCIN with funding from European Union NextGenerationEU (PRTR-C17.I1) and by The Basque Government under the IKUR program. The authors also thank the project BIDEKO, funded by MCIN/AEI, NextGenerationEU, PRTR. This work was also supported by the Basque Government (IT1658-22) and Grant PID2021-124294OB-C22 funded by MCI/AEI10.13039/501100011033 and by "ERDF A way of making Europe". J.U. thanks the University of the Basque Country for her fellowship (ESPDOC21/74).

References

[1] I. D'Adamo, M. Gastaldi, Perspectives and challenges on sustainability: drivers, opportunities and policy implications in universities, Sustainability 15 (4) (2023) 3564.
[2] S. Jessel, S. Sawyer, D. Hernández, Energy, poverty, and health in climate change: a comprehensive review of an emerging literature, Front. Public Health (2019) 357.
[3] M.K. Anser, et al., Impact of fossil fuels, renewable energy consumption and industrial growth on carbon emissions in Latin American and Caribbean economies, Atmósfera 33 (3) (2020) 201–213.
[4] E.A. Moallemi, et al., Local Agenda 2030 for sustainable development, The Lancet Planetary Health 3 (6) (2019) e240–e241.
[5] K. Baz, et al., Asymmetric impact of fossil fuel and renewable energy consumption on economic growth: a nonlinear technique, Energy 226 (2021), 120357.
[6] A. Kalair, et al., Role of energy storage systems in energy transition from fossil fuels to renewables, Energy Storage 3 (1) (2021), e135.
[7] C.M. Costa, et al., Recycling and environmental issues of lithium-ion batteries: advances, challenges and opportunities, Energy Storage Materials 37 (2021) 433–465.
[8] C. Costa, E. Lizundia, S. Lanceros-Méndez, Polymers for advanced lithium-ion batteries: state of the art and future needs on polymers for the different battery components, Prog. Energy Combust. Sci. 79 (2020), 100846.
[9] Y.K. Lee, The effect of active material, conductive additives, and binder in a cathode composite electrode on battery performance, Energies 12 (4) (2019) 658.
[10] B. Ramasubramanian, et al., Recent development in carbon-LiFePO4 cathodes for lithium-ion batteries: a mini review, Batteries 8 (10) (2022) 133.
[11] S. Liu, et al., Reviving the lithium-manganese-based layered oxide cathodes for lithium-ion batteries, Matter 4 (5) (2021) 1511–1527.
[12] S. Su, et al., Progress and perspective of the cathode/electrolyte interface construction in all-solid-state lithium batteries, Carbon Energy 3 (6) (2021) 866–894.
[13] M. Al Hassan, et al., Emergence of graphene as a promising anode material for rechargeable batteries: a review, Materials Today Chemistry 11 (2019) 225–243.
[14] K. Feng, et al., Silicon-based anodes for lithium-ion batteries: from fundamentals to practical applications, Small 14 (8) (2018) 1702737.
[15] C.M. Costa, S. Lanceros-Mendez, Recent advances on battery separators based on poly (vinylidene fluoride) and its copolymers for lithium-ion battery applications, Curr. Opin. Electrochem. 29 (2021), 100752.
[16] Y. Chen, et al., Oriented carbon fiber/PEO functional modified polyethylene separator for high-performance lithium metal batteries, Mater. Lett. 332 (2023), 133511.
[17] M.M. Rahman, et al., High temperature and high rate lithium-ion batteries with boron nitride nanotubes coated polypropylene separators, Energy Storage Materials 19 (2019) 352–359.
[18] Y. Zhao, et al., In situ construction channels of lithium-ion fast transport and uniform deposition to ensure safe high-performance solid batteries, Small 19 (39) (2023) 2301572.
[19] X. He, et al., Tuning interface lithiophobicity for lithium metal solid-state batteries, ACS Energy Lett. 7 (1) (2022) 131–139.
[20] L. Li, et al., Improving fast and safe transfer of lithium ions in solid-state lithium batteries by porosity and channel structure of polymer electrolyte, ACS Appl. Mater. Interfaces 13 (41) (2021) 48525–48535.
[21] A. Ojanguren, et al., Stable Na electrodeposition enabled by agarose-based water-soluble sodium ion battery separators, ACS Appl. Mater. Interfaces 13 (18) (2021) 21250–21260.
[22] O. Olatunji, Natural Polymers: Industry Techniques and Applications, Springer, 2015.
[23] A. Reizabal, et al., Silk fibroin and sericin polymer blends for sustainable battery separators, J. Colloid Interface Sci. 611 (2022) 366–376.
[24] J.P. Serra, et al., Sustainable lithium-ion battery separator membranes based on carrageenan biopolymer, Advanced Sustainable Systems 6 (12) (2022) 2200279.
[25] Q. Song, et al., Thermally stable, nano-porous and eco-friendly sodium alginate/attapulgite separator for lithium-ion batteries, Energy Storage Materials 22 (2019) 48–56.
[26] J. Barbosa, et al., Lithium-ion battery separator membranes based on poly (L-lactic acid) biopolymer, Materials Today Energy 18 (2020), 100494.
[27] D. Lv, et al., Pure cellulose lithium-ion battery separator with tunable pore size and improved working stability by cellulose nanofibrils, Carbohydr. Polym. 251 (2021), 116975.
[28] Y.B. Pottathara, et al., Chitin and chitosan composites for wearable electronics and energy storage devices, in: Handbook of Chitin and Chitosan, Elsevier, 2020, pp. 71–88.
[29] J. Wang, et al., Converting soy protein isolate into biomass-based polymer electrolyte by grafting modification for high-performance supercapacitors, Int. J. Biol. Macromol. 209 (2022) 268–278.
[30] M. Razmkhah, et al., Facile technique for wool coloration via locally forming of nano selenium photocatalyst imparting antibacterial and UV protection properties, J. Ind. Eng. Chem. 101 (2021) 153–164.
[31] A.N.M.A. Haque, et al., Thermally stable micro-sized silica-modified wool powder from one-step alkaline treatment, Powder Technol. 404 (2022), 117517.
[32] R.S. Pinto, et al., Direct-ink-writing of electroactive polymers for sensing and energy storage applications, Macromol. Mater. Eng. 306 (11) (2021) 2100372.
[33] S. Luiso, P. Fedkiw, Lithium-ion battery separators: recent developments and state of art, Current Opinion in Electrochemistry 20 (2020) 99–107.
[34] K. Rafiz, D.R.L. Murali, J.Y. Lin, Suppressing lithium dendrite growth on lithium-ion/metal batteries by a tortuously porous γ-alumina separator, Electrochim. Acta 421 (2022), 140478.
[35] S. Zhang, et al., Multifunctional electrode design consisting of 3D porous separator modulated with patterned anode for high-performance dual-ion batteries, Adv. Funct. Mater. 27 (39) (2017) 1703035.
[36] K. Wang, et al., Tough and strong soy protein film by integrating CNFs and MXene with photothermal conversion and UV-blocking performance, Cellulose 29 (17) (2022) 9235–9249.
[37] E.M. Masoud, et al., Gel P (VdF/HFP)/PVAc/lithium hexafluorophosphate composite electrolyte containing nano ZnO filler for lithium ion batteries application: effect of nano filler concentration on structure, thermal stability and transport properties, Polym. Test. 56 (2016) 277–286.
[38] T. Wang, et al., Development of proteins for high-performance energy storage devices: opportunities, challenges, and strategies, Adv. Energy Mater. 12 (44) (2022) 2202568.
[39] R. Afkhami, et al., Improvement of heat-induced nanofibrils formation of soy protein isolate through NaCl and microwave, Food Hydrocoll. 139 (2023), 108443.
[40] T. Garrido, et al., Chicken feathers as a natural source of sulphur to develop sustainable protein films with enhanced properties, Int. J. Biol. Macromol. 106 (2018) 523–531.
[41] Z. Wei, et al., Soy protein amyloid fibril scaffold for cultivated meat application, ACS Appl. Mater. Interfaces 15 (12) (2023) 15108–15119.
[42] P. Guerrero, K. De la Caba, Thermal and mechanical properties of soy protein films processed at different pH by compression, J. Food Eng. 100 (2) (2010) 261–269.
[43] Y. Xu, et al., Preparation of a moderate viscosity, high performance and adequately-stabilized soy protein-based adhesive via recombination of protein molecules, J. Clean. Prod. 255 (2020), 120303.
[44] Z. Lu, et al., Polyimide separators for rechargeable batteries, J. Energy Chem. 58 (2021) 170–197.
[45] S. Dai, et al., Soy protein isolate-catechin non-covalent and covalent complexes: focus on structure, aggregation, stability and in vitro digestion characteristics, Food Hydrocoll. 135 (2023), 108108.
[46] X. Xu, et al., Preparation and properties of electrospun soy protein isolate/polyethylene oxide nanofiber membranes, ACS Appl. Mater. Interfaces 4 (8) (2012) 4331–4337.
[47] J. Uranga, et al., Compression molded soy protein films with exopolysaccharides produced by cider lactic acid bacteria, Polymers 12 (9) (2020) 2106.
[48] N.K. Kim, R.J.T. Lin, D. Bhattacharyya, Extruded short wool fibre composites: mechanical and fire retardant properties, Compos. Part B Eng. 67 (2014) 472–480.
[49] B.-Y. Chang, S.-M. Park, Electrochemical impedance spectroscopy, Annu. Rev. Anal. Chem. 3 (1) (2010) 207–229.
[50] C.M. Costa, M.M. Silva, S. Lanceros-Méndez, Battery separators based on vinylidene fluoride (VDF) polymers and copolymers for lithium ion battery applications, RSC Adv. 3 (29) (2013) 11404–11417.
[51] C. Charton, et al., Reactivity of succinic anhydride at lithium and graphite electrodes, J. Electrochem. Soc. 164 (7) (2017) A1454.